Arch. Metall. Mater. **63** (2018), 1, 329-336

DOI: 10.24425/118945

Q. YUE*, X. PEI,* C. ZHANG*, X. WANG**#

MAGNETOHYDRODYNAMIC CALCULATION ON DOUBLE-LOOP CHANNEL INDUCTION TUNDISH

A mathematical model is developed to investigate the electromagnetic induction heating in a continuous casting tundish with the double-loop inductor. Maxwell's equations are solved using finite element method to obtain the magnetic flux density, electromagnetic force, and Joule heating. Results show that the induced current through the two channels generates a current loop. The electromagnetic force points to the center of the channel, thus generating a pinch effect on the molten steel. With the skin effect and proximity effect, Joule heating rate reaches its maximum and minimum values at the corners and the center of the cross-section area respectively. Power ampere-turn has a significant influence on the electromagnetic force and Joule heating density. As ampere-turns vary from 3.6×10^4 to 2.16×10^5, Joule heating rate increases from 2.4 MW m^{-3} to 85 MW m^{-3}. Electromagnetic force also increases from 8×10^4 N m^{-3} to 3×10^6 N m^{-3} in the center axis line of the channel. The present work reveals the relationship between magnetic flux density and electromagnetic force. The results will be helpful in adjusting the electromagnetic field in channel-induction furnaces and modifying the design of channel parameters.

Keywords: induction heating, electromagnetic field, channel, tundish

1. Introduction

The continuous casting tundish is widely utilized in the steelmaking industry. The aim of tundish metallurgy is to increase the molten steel mean residence time, decrease dead volume fraction, enhance inclusion removal, and promote molten steel temperature and composition homogenization [1,2]. Various flow control devices, such as dams, weirs [3-5] and other turbulence inhibitors [6,7], have been designed to improve the molten steel quality and thus obtain the ideal molten steel flow characteristic in tundish. The distribution of molten steel temperature is also critical to the final steel quality. Given the heat transfer between molten steel and its walls, the molten steel temperature is non-isothermal, especially on the free surface of the molten steel top. The molten steel casting temperature is higher than the melting point. Tundish with induction heating [8] and plasma heating [9,10] has been developed to improve molten steel temperature. As a result, the above mentioned problem is resolved and low superheat and constant temperature casting are achieved. The inductor-induced eddy currents in the molten steel generate Joule heating, thus leading to the rapid increase of molten steel temperature [11].

Induction heating has high efficiency, low oxide, good degassing, and low energy cost [12-14]; hence, this technology has been extensively applied for aluminum alloy and molten steel melting, and has attracted much attention [15-19]. Induction heating is applied to metallic melts since the pioneering work of Szekely [20] on coreless furnaces. In their mathematical models, electromagnetic body force and velocity field were obtained by solving Maxwell's equation, Navier-Stokes equation, turbulent energy, and turbulent energy dissipation rate equation for the turbulence model. These calculation results are important to understand the melt fluid flow phenomenon under electromagnetic field. Vives [21-22] used a cold, physical model experiment to investigate three-dimensional (3-D) electromagnetic and fluid flow phenomena. A four-tenth-scale channel furnace with a complete geometry similarity is adopted, where mercury is used as model melt. In their work, the presence of solid material, the possible cavitation phenomenon, and the velocity field is considered. On this condition, current density, magnetic field, electromagnetic force field was measured. According to their results, the magnitude and direction of flow vary several times in 1 min. This finding shows that the transverse fluid motion through the channel is very unstable. The mean electromagnetic force density ($J\times B$) is approximately 10^3 N m^{-3}, while the force can be estimated in the order of 10^7 N m^{-3} in the case of a large furnace. The buoyance force was considered insignificant to avoid superheating the bath, and the channel legs were cooled by water. Moreover, investigations [23-25] consisting of electromagnetic and hydrodynamic melt flow have been conducted to better understand the electromagnetic field and flow characteristics. Based on the experiment of tundish with channel-type

* SCHOOL OF METALLURGY ENGINEERING, ANHUI UNIVERSITY OF TECHNOLOGY, MA' ANSHAN 243002, CHINA
** COLLEGE OF MECHANICAL ENGINEERING, ANHUI UNIVERSITY OF TECHNOLOGY, MAANSHAN ANHUI 243002, CHINA
# Corresponding author: yueqneu@163.com

electromagnetic induction heating, Yoshii et al. [16] reported that the number of subsurface inclusions in stainless steel slab cast decreases from one-fourth to one-half compared with that of slab cast without induction heating at unsteady or steady state. Taniguchi [26,27] proposed that the pinch force generated by imposing an electrical current on molten metals is efficient for inclusion removal from molten steel. However, the Joule heating generation has been always been neglected. Recently, Wang [8] developed a numerical model to predict electromagnetic field, flow field, and heat transfer in tundish. Their study focused on the Joule heating and temperature distribution in a sample tundish with induction heating.

In the present study, a finite element model is developed to investigate the electromagnetic induction heating in industrial seven-strand slab continuous casting tundish with the double-loop inductor. The electromagnetic field intensity, Joule heating, and electromagnetic forces are discussed. The study on a straight channel is conducted with the effect of frequency and power. The evaluation of numerical data is helpful to adjust the electromagnetic field in channel-induction furnaces and modify the design of channel parameters.

2. Electric magnetic modeling

The loop current in molten steel is induced because the flux of the primary coil periodically changes and the molten steel is conductive. The loop current leads to two facts. On the one hand, given the existence of steel molten resistance, the loop current generates Joule heating, which can directly heat the molten steel. On the other hand, the loop current leads to the induction electromotive force. Especially, for the double-channel induction heating tundish, the existence of a two-level loop through electromagnetic induction transmission results in the level circuit of electric energy in molten steel. This feature is the basic principle of channel induction heating, which is characterized by high thermal efficiency.

Molten steel is poured into the pouring chamber of the tundish from the ladle. Joule heating is generated through the channel of its own induction current heating. The heated molten steel from the tundish channel flows into the casting chamber. The molten steel in channels is heated in a short time, and the temperature of molten steel in the casting chamber is increased by the flow of molten steel. The geometry of a seven-strand tundish with channel-type induction heating is shown in Fig. 1. The system is constructed based on a channel-type industrial seven-strand tundish. The 3-D structure of a tundish consists of tundish main body, channel, coil, and iron core. The air bag is excluded.

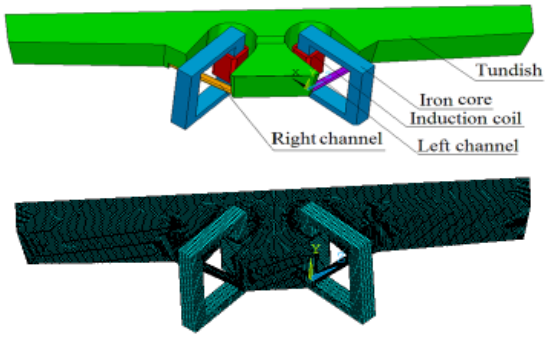

Fig. 1. Tundish with straight channel induction heating geometry and mesh

Electromagnetic fields are governed by the following Maxwell's equations:

$$\nabla \times H = J + \frac{\partial D}{\partial t} \tag{1}$$

$$\nabla \times E = -\frac{\partial B}{\partial t} \tag{2}$$

$$\nabla \times B = 0 \tag{3}$$

$$\nabla \times D = \rho_e \tag{4}$$

The continuity equation is obtained using the divergence of both sides of Equation 5.

$$\nabla \times J = \frac{\partial \rho}{\partial t} \tag{5}$$

The continuity equation must be satisfied to properly set the Maxwell's equations. Thus, the J should be considered. The above field equations are supplemented by the constitutive relation, which describes the behavior of electromagnetic materials. For saturated material without permanent magnets, the following additional conditions are induced.

$$B = \mu H = \mu_0 \mu_r H \tag{6}$$

The constitutive relations for the related electric fields are

$$D = \varepsilon E = \varepsilon_0 \varepsilon_r E \tag{7}$$

$$J = \sigma[E + (u \times B)] \tag{8}$$

where μ is the magnetic permeability matrix, and is a function of ω in general. The Joule heating power density produced by the interaction of induced current and molten steel is expressed by

$$\omega = \frac{Q_j}{t} = \frac{(J^2/\sigma)\cdot t}{t} = \sigma E^2 \tag{9}$$

The time-averaged electromagnetic force is expressed as follows:

$$F = J \times B \tag{10}$$

The finite element volume of channel, coil, and iron core are adjusted manually to ensure the mesh quality. Hexahedron cell is used for the channel, coil, and iron core. Tundish main body and air bag mesh are used in a tetrahedron. A total of 90,500 cells are used. Fig. 1b shows the finite element model for the tundish with an induction heating system.

The magnetic scalar potential method is used to solve the electromagnetic field and Joule heating. Magnetic current density, electrical magnetic flux density, and electromagnetic force are calculated using the magnetic scalar potential method. Joule

heating is calculated using the current density. In this calculation, the electric conductivity of 175 s m^{-1} is used. The air bag surfaces are set with the magnetic flux parallel condition.

3. Validation of mathematical model

In this work, a mathematical model is proposed to study the magnetic flux density and electromagnetic force in a tundish with double-loop channel induction heating. To validate the mathematical model, the experimental validation of the mathematical model is established by comparing it with the experimental data reported in literature.

The data are acquired from the electromagnetic field of a channel induction furnace in the laboratory model in Vives and Ricou's [21] experiment. Their system with electromagnetic loop is similar to the tundish with induction heating in the present work. The same channel geometry, ampere-turns, and frequency are applied to the apparatus with induction heating in the validation work. The predicted results include the electromagnetic force in the lateral and central channels.

Fig. 2 shows the validation of the electromagnetic model. Fig. 2a shows the predicted electromagnetic force vector at the center plane in the left channel (diameter is 6 cm), and Fig. 2b shows the predicted electromagnetic force vector at the center plane in the central channel (diameter is 8 cm). Fig. 2c shows the comparison of electromagnetic force at the center plane in the left channel, and Fig. 2d shows the comparison of electromagnetic force at the center plane in the right channel. The value of magnetic flux density and predicted electromagnetic force agree well with the values and distribution measured in the experiments.

4. Results and discussion

To visualize the electromagnetic force, electric magnetic flux density, and Joule heating inside the channels, five planes and four lines were selected, as illustrated in Fig. 3. Four planes were parallel to the channel horizontal cross-section surfaces, and four lines were selected along the channel vertical dimension. The coordinate system is also presented in Fig. 3.

The predicted magnetic flux density field of different planes in the left channel of tundish with 73000 power induction heating power is shown in Fig. 4. Figs. 4a-d are presented for planes 1, 2, 3 and 4, respectively. The direction of magnetic flux density is counterclockwise according to the right-hand rule of applied current. The arrows reveal the direction and magnitude of the value of the magnetic field. The ideal case of magnetic field passing through a cylinder is characterized by concentric circular magnetic fields. Notably, the magnetic field distribution varies insignificantly with z axis direction in the vertical planes 1 to 4. The magnetic flux density is eccentric and non-uniform along the radial direction. The maximum value of magnetic flux density is nearly 0.032 T.

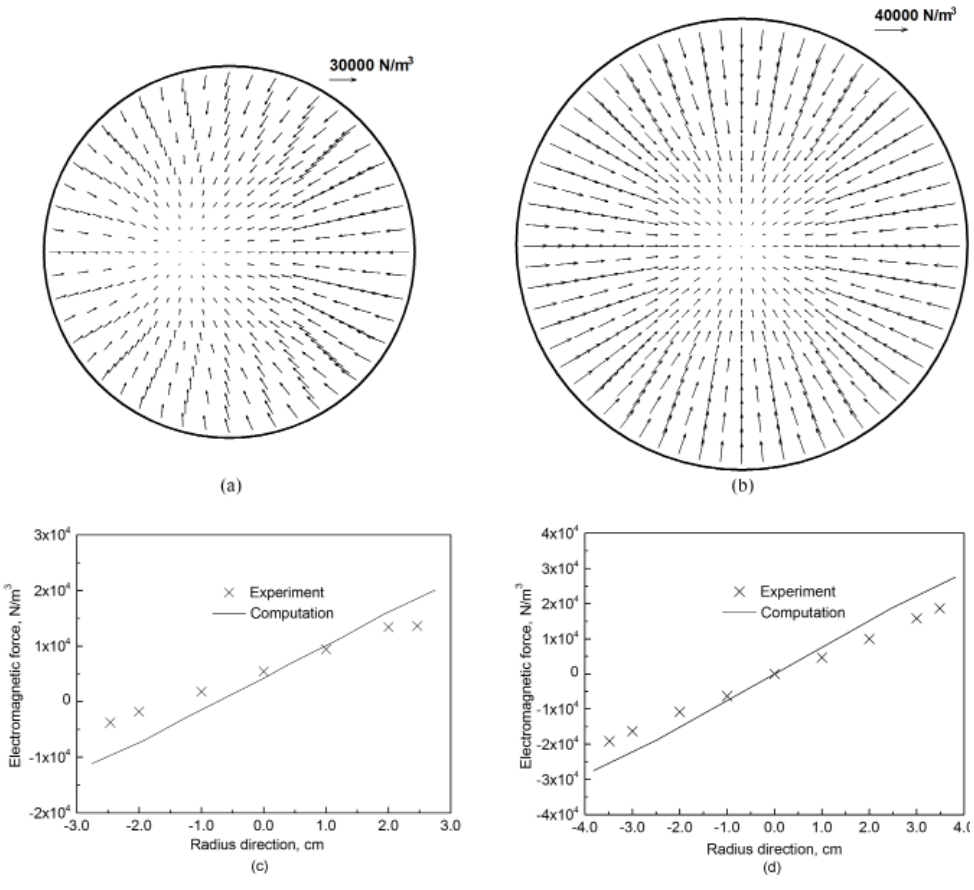

Fig. 2. Validation of the electromagnetic model

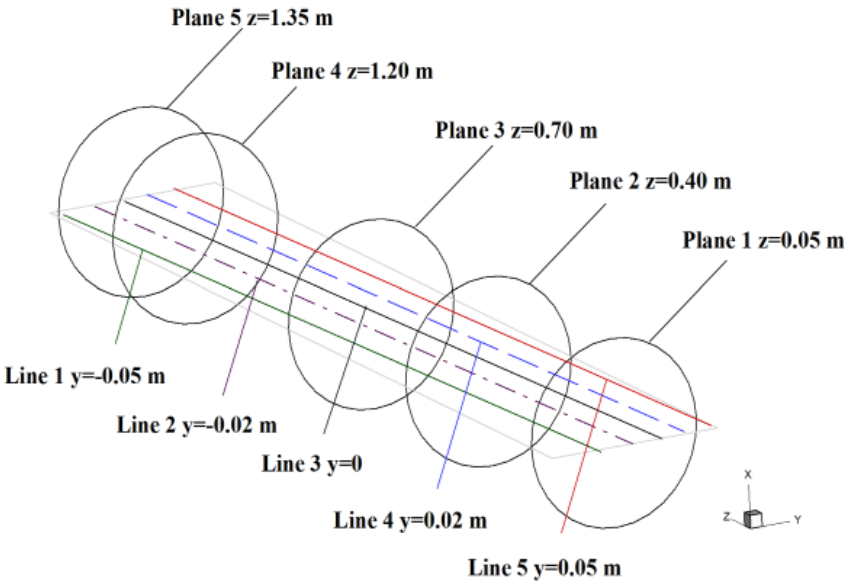

Fig. 3. Position of investigated planes and lines in the left channel

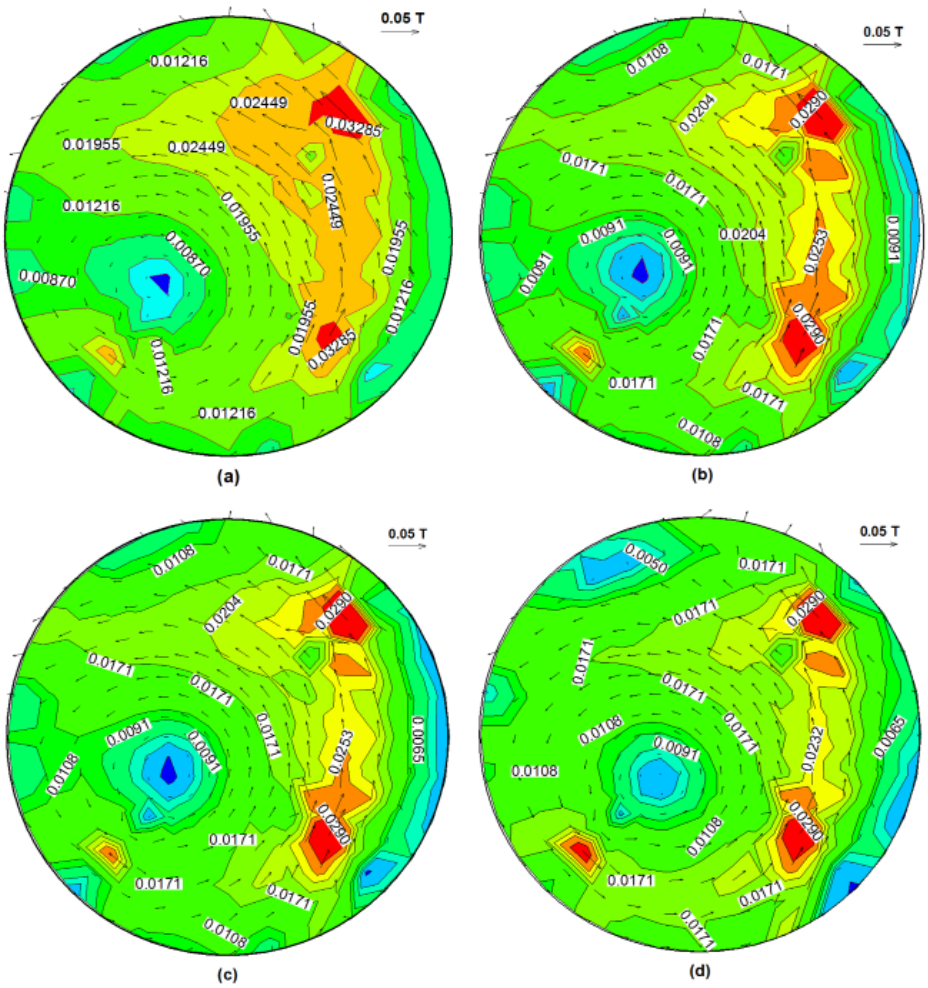

Fig. 4. Magnetic flux density in planes 1 to 4

Fig. 5 displays the variations of magnetic flux density of 50 Hz frequency at different vertical locations. The channel diameter is 0.16 m. The left channel coordinates range from –0.08 m to 0.08 m. Owing to the proximity effect, the maximum value is located close to the coil part of the channel. The magnetic flux density is different along lines 1 to 5. The region near the iron core is larger than the other area because of its considerable relative magnetic permeability. The magnetic field

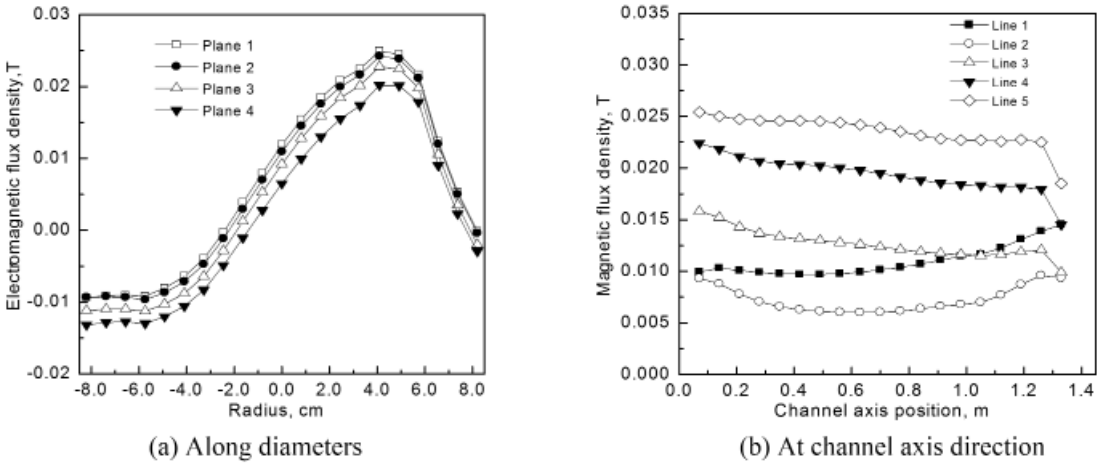

Fig. 5. Magnetic flux density in lines 1 to 5 at diameters channel axis direction

is enhanced inside the closed region from the iron core, and thus, the magnetic field distribution is eccentric. The magnetic field varies in magnitude along circular lines located in the horizontal cross section. Magnetic field distributions in the horizontal cross section also vary insignificantly along the channel axis direction.

The mean electromagnetic force density $J \times B$ is considered inside the channel. Fig. 6 shows the electromagnetic force distribution at the horizontal cross section. The magnitude of the electromagnetic force is nearly on the order of 10^5 N m^{-3}, and the direction of the electromagnetic force is inward in all positions. The electromagnetic force central point is not the geometric center of the channel cross section. Given the asymmetrical flux density of the induced current and magnetic field, the electromagnetic force field is also asymmetrical. The magnetic force

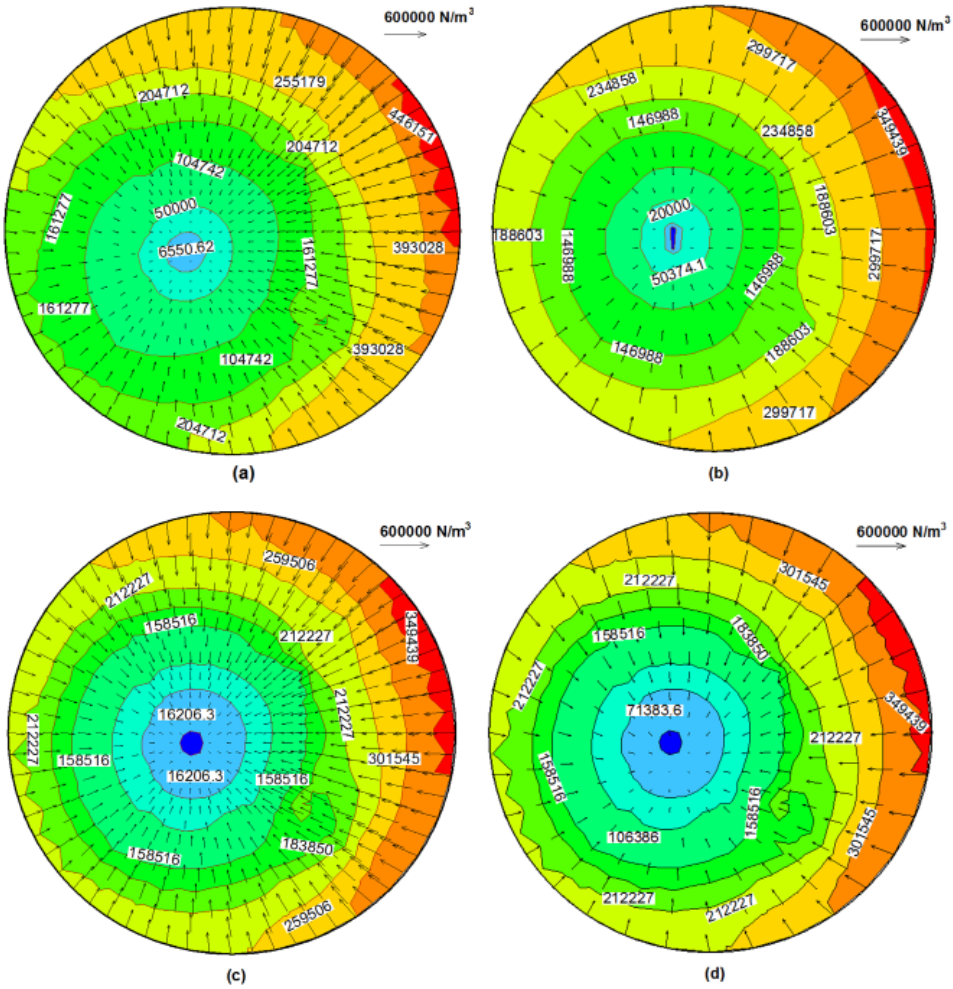

Fig. 6. Electromagnetic forces in planes 1 to 4

is also not pointing to the center of the horizontal cross section. The electromagnetic forces along the diameters are shown in Fig. 7a. The electromagnetic force closer to the induction coil along the channel side is higher than that on the other side. The eccentric electromagnetic force may generate a pinch effect on the molten steel. The pinch effect generated by the eccentric electromagnetic force will produce a rotary motion when the steel flows through the channel. The molten steel is extruded by the electromagnetic force when it flows through the channels. Collision and coagulation between small non-metallic inclusions expect in the oscillatory pinch field. The electromagnetic body force insulating inside the inclusion is close to zero. With the pinch effect, electrically non-conductive inclusions suspended in the molten steel will be squeezed out from the molten steel. The distribution of electromagnetic force in vertical lines is also the same. The molten steel acts on by an eccentric force.

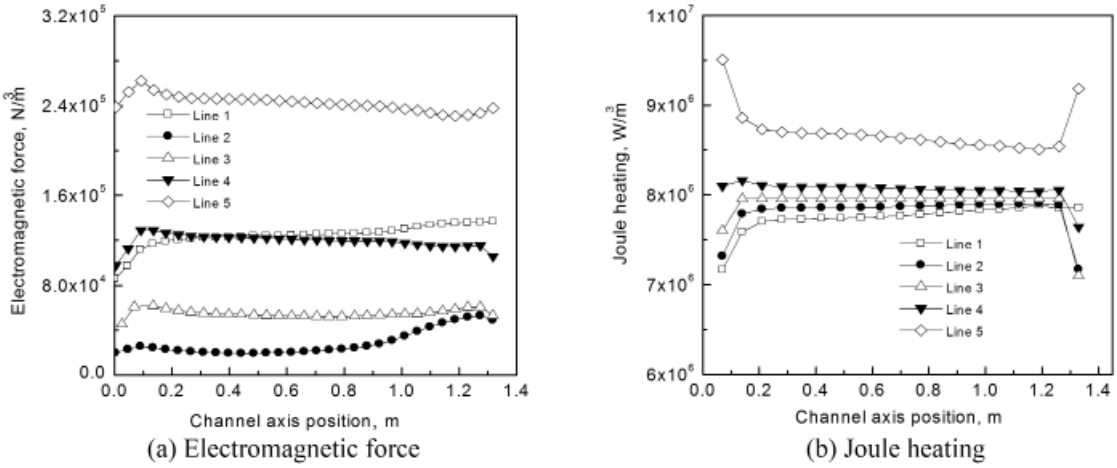

Fig. 7. Electromagnetic force and Joule heating in lines 1 to 5

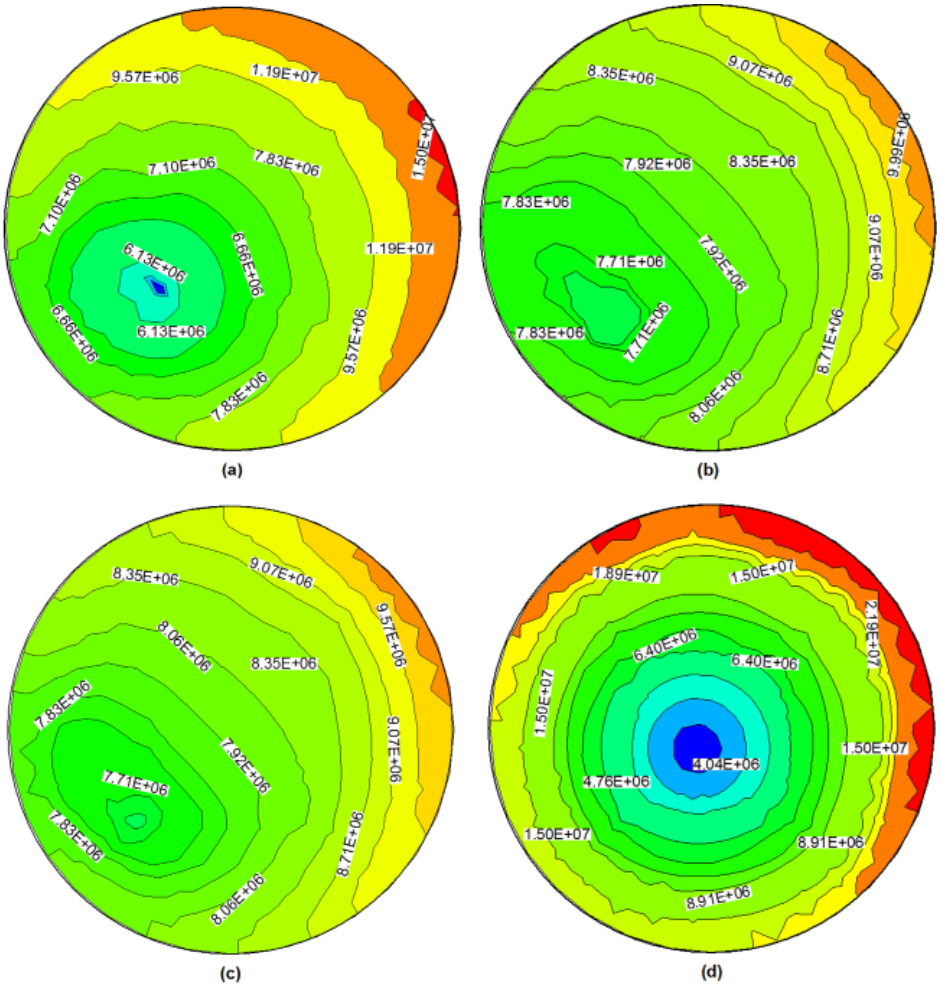

Fig. 8. Joule heating in planes 1 to 4

One of the most important roles of the inductor is to produce the necessary Joule heating to heat the molten steel. Type channel tundish induction heating can effectively compensate for the heat loss for molten steel; this compensation keeps the temperature of molten steel constant. Thus, the quality of steel products is improved. Given the large channel-induced current density, the Joule heating is generated mainly in the two channels. The maximum Joule heating occurs at the junction of the channel and the distribution chamber and reaches up to 0.9×10^7 W m^{-3}. The minimum occurs in the central portion of the channels. The molten steel is heated when it flows through the channel. Joule heating per unit volume is generated by the current density and is inversely proportional to the electrical conductivity of molten steel. Hence, Joule heating density is similar to the induced current density. Fig. 8 shows the predicted distribution of Joule heating. The maximum current density occurs at the periphery of the channel, as shown in this figure. The maximum Joule heating density at the line in the horizontal cross section is 2.19×10^7 W m^{-3}. This value near the Joule heating coil is large, which is due to the eddy currents induced by the skin effect and proximity effect.

As can be seen from the data in Fig. 9, the induced current and magnetic flux density distribution profiles are obtained with five Ampere-turns. The value of the magnetic flux density at the channel axis increases with an increase of power.

The induction electric current on the cross-section changes notably with the increase of power Ampere-turns. For example, when power increases from 3.6×10^4 to 2.16×10^5, the induction electric current varies from 5.0×10^5 to 3×10^6 A m^{-2}; the magnetic flux density in the center axis line of the channel increases from 0.004 T to 0.03 T. The electromagnetic field is strengthened by the high permeable laminated core. Joule heating is caused by the corresponding losses of electrical energy. The eddy loss of the iron core is not considered in this work. As shown in Fig. 9, the Joule heating and electromagnetic force of molten steel at the tundish channel also increase with the increase of power. The power plays a critical role in determining the Joule heating and electromagnetic force in the tundish channel as a result of electromagnetic induction. The Joule heating rate clearly improves with the increase of power. When power varies from 3.6×10^4 ampere-turns to 2.16×10^5 ampere-turns, the Joule heating rate increases from 2.4 MW m^{-3} to 85 MW m^{-3}, and the electromagnetic force rises from 8×10^4 to 3×10^6 N m^{-3} in the center axis line of the channel.

5. Summary

This study performs a numerical simulation to investigate the 3-D aspects of the electromagnetic phenomena that occur in the continuous casting tundish with double-loop channel inductor heating. The study also examines the important parameters of the influence of the magnetic flux density, electromagnetic force,

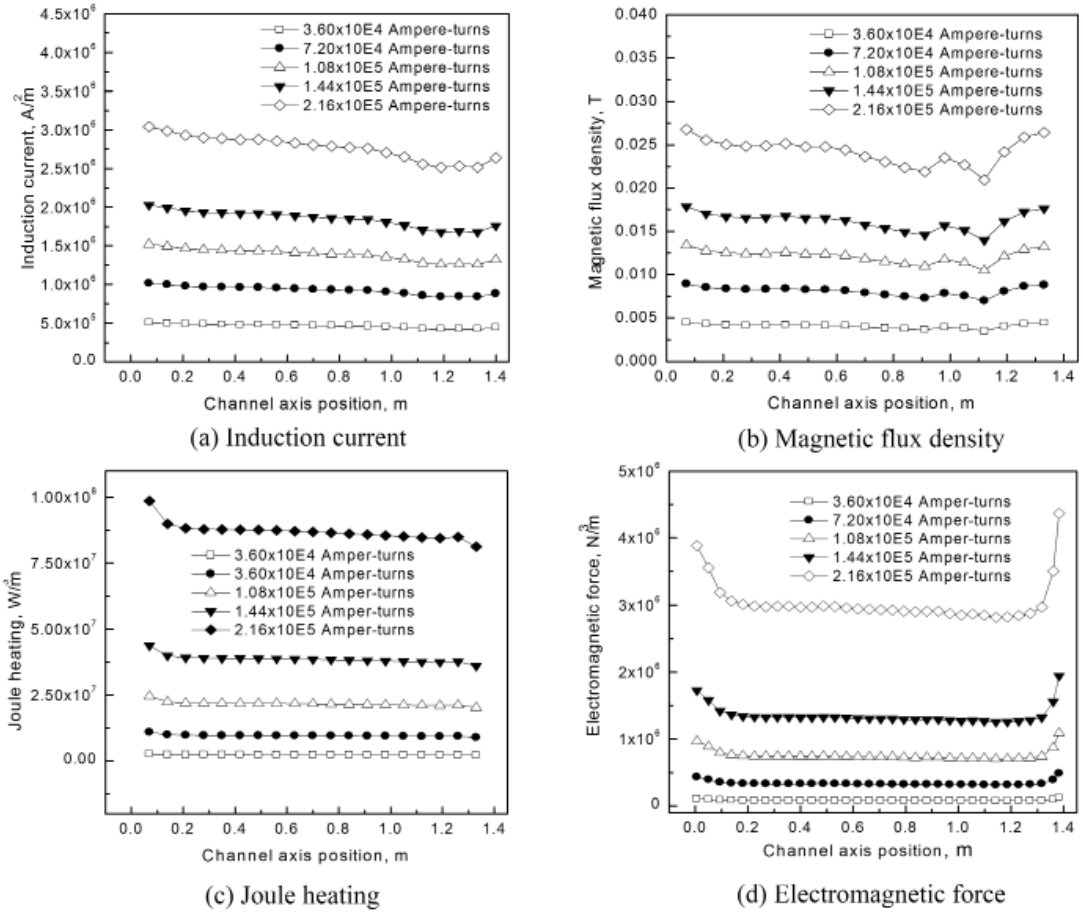

Fig. 9. Magnetic variable at line of y = 0.05 m under different condition of Power

and Joule heating, all of which are analyzed by mathematical modeling. The magnetic leaks coming mainly from the primary coils are not considered in the study. The following conclusions can be drawn:

(1) Induced current loop through the two tundish chambers along two channels. The induced current density in the channel is larger than other regions because of the skin effect and the proximity effect. The induced current density in the passage near the induction coil is greater than that of others.

(2) The electromagnetic force is directed inward; the central point is not the geometric center of the channel cross section. Given the uneven distribution of the induced current, the magnetic force does not point to the center of the horizontal cross section. The electromagnetic force that produces a "pinch effect" for the molten steel is eccentric. The electromagnetic forces produce rotary motion through the eccentric electromagnetic force when the molten steel flows through the channel.

(3) High power is beneficial to the Joule heating rate and electromagnetic force. The power Ampere-turns play an important role in the performance of the double-loop channel inductor.

(4) The 3-D electromagnetic modeling can be used in industrial tundish to predict the Joule heating and electromagnetic forces and optimize the induction heating parameters.

Acknowledgements

This work was supported by grants from the Anhui University Provincial Natural Science Research Key Project (KJ2016A101), the National Natural Science Foundation of China (51774004) and Provincial College Students Innovation and entrepreneurship training program in 2014 (201410360132).

Nomenclature

B – Magnetic flux density [T],
D – Electric displacement [A/m^2],
E – Induced electromotive force [V],
F – Magnetic force density [N m^{-3}],
Q_j – Joule heating energy [J],
J – Current density [A m^{-2}],
H – Magnetic field intensity [A m^{-1}],
t – Time [s].

Greek

∇ – Different operator [–],
ε – Dielectric constant [–],
ε_0 – Vacuum dielectric constant [–],
ε_r – Relative dielectric constant [–],
μ – Magnetic permeability (H/m),
μ_0 – Vacuum magnetic permeability [H m^{-1}],
μ_r – Relative magnetic permeability [–],
ρ_e – Electric density [C m^{-2}],
ω – Joule heating power density [W m^{-3}],
σ – Electric conductivity [s m^{-1}].

REFERENCES

[1] Y. Sahai, Mater. Trans. B 1-12, (2016).
[2] A. Cwudziński, Ironmak. Steelmak. **42**, 132-138 (2015).
[3] K. Chattopadhyay, M. Isac, R.I.L. Guthrie, ISIJ Int. **50**, 331-348 (2010).
[4] T. Merder, Archives of Metallurgy & Materials **58**, 1111-1117 (2013).
[5] A. Cwudziński, Steel Res. Int. **81**, 123-131 (2010).
[6] G. Solorio-diaz, R.D. Morales, Int. J. Heat Mass. Tran. **48**, 3574-3590 (2005).
[7] Y. Miki, S. Ogura, T. Fujii, Kawasaki Steel Technical Report, Japan, 67-73 (1996).
[8] Q. Wang, B.K. Li, F. Tsukihashi, ISIJ Int. **54**, 311-320 (2014).
[9] M.A.B. N-Meza, J.J. Barreto-Sandoval, R.D. Morales, Mater. Trans. B **31**, 63-74 (2000).
[10] J.J. Barreto-Sandoval, A.W.D. Hills, M.A. Barron-Me, R.D. Morales, ISIJ Int. **36**, 1174-1183 (1996).
[11] K. Umetsu, Y. Tomizawa, K. Myojin, The 5th International Symposium on Electromagnetic Processing of Materials, Sendai, Japan, 485-489 (2006).
[12] J.L. Meyer, F. Durand, R. Ricou, C. Vives, Mater. Trans. B **15**, 471-478 (1984).
[13] Y. Kishida, K. Takedai, K. Miyoshino, E. Takeuchi, ISIJ Int. **30**, 34-40 (1990).
[14] J.I. Ghojel, R.N. Ibrahim, Mater. Process Tech. 386-391 (2004).
[15] C. Vives, Metall. Mater. Trans. B, 631-638 (1989).
[16] Y. Yoshii, T. Nozaki, Y. Habu, T. Ueda, A. Harita, M. Sakurai, Tetsu-to-Hagane **71**, 1474-1481 (1985).
[17] R. Schwarze, F. Obermeier, Model Simul. Mater. Sc. **12**, 985-993 (2004).
[18] A. Umbrashko, E. Baake, B. Nacke, A. Jakovics, Metall. Mater. Trans. B **37**, 831-838 (2006).
[19] J.I. Ghojel, Prog. Comput. Fluid. Dy. **6**, 435-445(2006).
[20] J. Szekely, C.W. Chang, R.E. Ryan, Metall. Mater. Trans. B **8**, 333-338 (1977).
[21] C. Vives, R. Ricou, Metall. Mater. Trans. B **22**, 193-209 (1991).
[22] C. Vives, R. Ricou, Proceedings of the Sixth International Iron and Steel Congress, Nagoya, Japan, 307-489 (1990).
[23] A. Morost, J.C.R. Hunt, Int. J. Heat Mass. Tran. **31**, 1497-1515 (1988).
[24] A. Bermúdez, D. Gómez, M.C. Muñiz, P. Salgado, R. Vázquez, Appl. Numer. Math. **59**, 2082-2104 (2009).
[25] M. Kirpo, A. Jakovics, B. Nacke, E. Baake, M. angejrgen, Przegląd Elektrotechniczny **11**, 154-158 (2008).
[26] S. Taniguchi, J.K. Brimacombe, ISIJ Int. **34**, 722-731 (1994).
[27] S. Taniguchi, J.K. Brimacombe, Tetsu-to-Hagane. **81**, 24-28 (1994).